REPORT DOCUMENTATION PAGE

Form Approved OMB No. 0704-0188

Public reporting burden for this collection of information is estimated to average 1 hour per response, including the time for reviewing instructions, searching existing data sources, gathering and maintaining the data needed, and completing and reviewing the collection of information. Send comments regarding this burden estimate or any other aspect of this collection of information, including suggestions for reducing the burden, to Department of Defense, Washington Headquarters Services, Directorate for Information Operations and Reports (0704-0188), 1215 Jefferson Davis Highway, Suite 1204, Arlington, VA 22202-4302. Respondents should be aware that notwithstanding any other provision of law, no person shall be subject to any penalty for failing to comply with a collection of information if it does not display a currently valid OMB control number.
PLEASE DO NOT RETURN YOUR FORM TO THE ABOVE ADDRESS.

1. REPORT DATE *(DD-MM-YYYY)*	2. REPORT TYPE	3. DATES COVERED *(From – To)*
27-01-2007	Final Report	1 January 2006 - 26-Jul-07

4. TITLE AND SUBTITLE

Mechanisms of Recrystallization in Superalloys

5a. CONTRACT NUMBER
FA8655-06-M-4001

5b. GRANT NUMBER

5c. PROGRAM ELEMENT NUMBER

6. AUTHOR(S)

Dr. Frank J Montheillet

5d. PROJECT NUMBER

5d. TASK NUMBER

5e. WORK UNIT NUMBER

7. PERFORMING ORGANIZATION NAME(S) AND ADDRESS(ES)

Ecole des Mines de Saint-Etienne (ENSM-SE)
158, cours Fauriel
Saint-Etienne Cedex 2 42023
France

8. PERFORMING ORGANIZATION REPORT NUMBER

N/A

9. SPONSORING/MONITORING AGENCY NAME(S) AND ADDRESS(ES)

EOARD
PSC 821 BOX 14
FPO AE 09421-0014

10. SPONSOR/MONITOR'S ACRONYM(S)

11. SPONSOR/MONITOR'S REPORT NUMBER(S)
SPC 06-4001

12. DISTRIBUTION/AVAILABILITY STATEMENT

Approved for public release; distribution is unlimited.

13. SUPPLEMENTARY NOTES

14. ABSTRACT

This report results from a contract tasking Ecole des Mines de Saint-Etienne (ENSM-SE) as follows: The project will study the effects and influence of very low (50 -100 ppm) and very high (10-15%) niobium content in solid solution. Quantitative analysis of the stress-strain relationship will be conducted to determine stress-strain curves (up to large strains) at various temperatures and strain rates (typical ranges: 800 to 1000 °C, 0.01 to 1 s-1). Beyond the overall strain rate sensitivity (m) and apparent activation energy (Q), strain hardening (h) and dynamic recovery (r) parameters will be extracted from the data using one of the available physical equations. Evolutions of the above rheological parameters with Nb content for given straining conditions will therefore be deduced and compared with that of industrial grades. Electron Backscattering Diffraction imaging will be used to determine the Dynamic Recrystallization mechanisms operating in the various cases. Deformation microstructures will be characterized quantitatively (grain or crystallite size distributions, misorientation distributions, crystallographic texture). Such data will be put into correlation with the associated hot deformation flow stress (Derby diagrams). Two or three different states likely to be associated with precipitation of Ni3Nb will first be selected from the stress-strain curve shapes and micro-hardness measurements. Transmission Electron Microscopy will then be used to determine the nature, size, morphology and localization of the intermetallic (Ni3Nb) particles after straining followed by quench. In particular, their possible interactions with dislocations and grain boundaries will be analyzed.

15. SUBJECT TERMS

Microstructure, Superalloy, Metallic Materials

16. SECURITY CLASSIFICATION OF:			17. LIMITATION OF ABSTRACT	18, NUMBER OF PAGES	19a. NAME OF RESPONSIBLE PERSON
a. REPORT	b. ABSTRACT	c. THIS PAGE			WYNN SANDERS, Maj (S), USAF
UNCLAS	UNCLAS	UNCLAS	UL	32	19b. TELEPHONE NUMBER *(Include area code)* +44 (0)20 7514 3154

Ecole Nationale Supérieure des Mines
SAINT-ETIENNE

CENTRE NATIONAL DE LA RECHERCHE SCIENTIFIQUE

Center for Materials Science and Structures

Plasticity, Damage, and Corrosion of Materials
CNRS Laboratory

MECHANISMS OF RECRYSTALLIZATION IN SUPERALLOYS

EOARD Contract No. FA8655-06-M-4001

Final Report

F. Montheillet and J. Le Coze

January 2007

Research Project No FA8655-06-M-4001

APPENDIX

1 - The Contractor, Ecole des Mines de Saint-Etienne (ENSM-SE), hereby declares that, to the best of its knowledge and belief, the technical data delivered herewith under Contract No. FA8655-06-M-4001 is complete, accurate, and complies with all requirements of the contract.

2 - Acknowledgement of Sponsorship: Effort sponsored by the Air Force Office of Scientific Research, Air Force Material Command, USAF, under grant number FA8655-06-M-4001. The U.S. Government is authorized to reproduce and distribute reprints for Government purpose notwithstanding any copyright notation thereon.

3 - Disclaimer: The views and conclusions contained herein are those of the author and should not be interpreted as necessarily representing the official policies or endorsements, either expressed or implied, of the Air Force Office of Scientific Research or the U.S. Government.

4 - Disclosure of inventions: I certify that there were no subject inventions to declare during the performance of this grant.

Frank Montheillet
Directeur de Recherche au CNRS

CONTENTS

This work was carried out with the technical help of Mrs. Séverine Girard, Prisca Lévêque, Cécile Genevois, Marilyne Mondon, and Mr. Sébastien Saunier, who are gratefully acknowledged.

I. INTRODUCTION

The general purpose of the present program is to investigate the mechanisms of dynamic recrystallization occurring during hot working of nickel base superalloys. More specifically, the role of niobium additions either as solute element or in the form of intermetallic precipitates is addressed. To discard interactions with other additions or impurities present in the industrial alloys, model materials prepared from pure nickel and niobium are used.

Former research, carried out under EOARD contract No. FA8655-03-M-4061, has shown that solid solution niobium has a strong influence on the hot deformation of nickel, for weight concentrations less than 1 % [Montheillet et al., 2006]. Since such effects appeared to increase very quickly between 0 and 1000 ppm (0.1wt%), a first natural step was to investigate an alloy with very low Nb content, *viz.* Ni-0.01 wt%Nb (referred to here as Ni-0.01Nb). Two other alloys containing 10 wt%Nb (Ni-10Nb) and 15 wt%Nb (Ni-15Nb), respectively, were prepared as well, as described in Section II.

Stress-strain curves of the two alloys Ni-0.01Nb and Ni-10Nb were investigated by torsion tests at various strain rates within the hot forging temperature range, which allow large strain steady state flow stresses to be reached. However, only a few data were obtained from the last alloy Ni-15Nb, due to its limited forgeability. The rheological behaviour of the alloys was then characterized by the classical strain rate sensitivity and apparent activation energy parameters (Section III).

In Section IV, the stress-strain curves of pure nickel and Ni-Nb alloys containing 0.01 %, 0.1 %, 1 %, and 10 %Nb (referred to as Ni-0.01Nb, Ni-0.1Nb, Ni-1Nb, and Ni-10Nb, respectively) are analyzed according to the Yoshie-Laasraoui-Jonas flow rule. The classical "Derby relationship" between the steady state average grain size and flow stress is investigated for the same model alloys in Section V.

Finally, the above data are discussed and compared in Section VI.

II. PREPARATION OF MODEL HIGH PURITY BASE Ni-Nb ALLOYS

Three alloys were prepared using an induction melting device described elsewhere [Le Coze et al., 1995; Montheillet *et al.*, 2004]. Purification is performed by repeated melting under high purity argon-hydrogen atmosphere. The niobium and residual metalloid contents were measured by atomic absorption, spark emission spectroscopy, and inductive coupling plasma (optical emission spectroscopy, ICP-OES). The average results are given in Table I.

Table I. Chemical analyses of the alloys

Alloy	Nb (wt%)	C (ppm)	S (ppm)	O (ppm)	N (ppm)	Ni
Ni-0.01Nb	0.0105	5.5	5	4.5	1	Balance
Ni-10Nb	9.5	6	5	3.2	3	Balance
Ni-15Nb	15	4	4	9	4	Balance

Ingots of about 1.1 kg were hot forged at 1050 °C (furnace temperature) into cylindrical bars of diameter 16 mm and then reduced by swaging at the same temperature to a diameter of 10.7 mm. 13 torsion specimens of gauge length 27 mm and diameter 6 mm were then machined from each of the bars.

III. RHEOLOGICAL BEHAVIOUR OF THE Ni-0.01Nb, Ni-10Nb, and Ni-15Nb ALLOYS

For comparison with previous data, large strain hot torsion tests were carried out at the same temperatures and strain rates, according to Table II, except for Ni-15Nb (see III.3). All specimens were heated to the test temperature up to stabilization (≈ 15 min) and quenched using a room temperature flow of argon immediately after deformation to an outer strain of 5, where a steady state flow stress was clearly attained.

Table II. Temperature and strain rate conditions of the torsion tests carried out on pure Ni, Ni-0.01Nb, Ni-0.1Nb, Ni-1Nb, and Ni-10Nb

		Temperature (°C)				
		800	850	900	950	1000
Strain rate (s^{-1})	0.03	*		*		*
	0.10	*	*	*	*	*
	0.30	*		*		*

The above schedule was chosen to allow the determination of the strain rate sensitivity parameter at 800, 900, and 1000 °C and the apparent activation energy at 0.1 s^{-1} with a good accuracy.

The "engineering" strain rate sensitivity $\tilde{m} = \partial \ln \Gamma / \partial \ln \dot{N}$ was derived in a first step from the experimental data for N corresponding to the maximum torque ($\tilde{m}_M$) and for the steady state ($\tilde{m}_S$). Since the two values generally do not coincide and increase slightly with temperature, an overall average was used for deriving the flow stress according to the classical Fields and Backofen equation:

$$\sigma = \frac{\sqrt{3}\,\Gamma}{2\pi R_0^3}\left(3 + \tilde{m} + \tilde{n}\right) \qquad (1)$$

where R_0 is the outer radius of the specimen. In the above formula, the "engineering" strain hardening parameter $\tilde{n} = \partial \ln \Gamma / \partial \ln N$ was determined in turn from each of the $\Gamma - N$ curves using a smoothing and derivation procedure.

III.1. Ni-0.01 Alloy

The stress-strain curves of alloy Ni-0.01Nb are displayed in the three diagrams of Figure 1 for strain rates of 0.03, 0.1, and 0.3 s^{-1}, respectively. The overall shape of the curves is similar to that of pure nickel [Montheillet et al., 2006], but the flow stress is significantly higher. The oscillations following the peak flow stress are more visible than in Ni. In the latter case, these waves have been ascribed to possible artifacts, for instance the large initial grain size. In the present case, however, they could reflect grain size coarsening usually associated with multiple peak discontinuous dynamic recrystallization, although the initial grain size is likely to be quite large. This point should be checked in further work. Finally, the strain required to achieve flow stress steady state is larger than for pure nickel, which confirms that niobium solutes slows down the dynamic recrystallization process.

The strain rate sensitivity parameter m was determined at 800, 900 and 1000 °C for both the peak flow stress ($m_M = \partial \ln \sigma_M / \partial \ln \dot{\varepsilon}$) and the steady state flow stress ($m_S = \partial \ln \sigma_S / \partial \ln \dot{\varepsilon}$) from the $\log \sigma - \log \dot{\varepsilon}$ curves of Figure 2. Data reported in Table III show that m slightly increases with temperature, with average values m_M = 0.173 and m_S = 0.134 (very close to their "engineering" counterparts, $\tilde{m}_M$ and $\tilde{m}_S$, respectively). It is worth to note that m_S is significantly lower than m_M.

The apparent activation energy for deformation of the alloy was determined in turn for the peak flow stress (Q_M) and the steady state flow stress (Q_S) at a strain rate of 0.1 s^{-1} from the $\ln \sigma - 1/T$ plot of Figure 3. As it was already noticed for Ni and the alloys Ni-0.1Nb and Ni-1Nb, the five available points are remarkably aligned in this diagram [Montheillet et al., 2006]. Since the slope of the curve is $\partial \ln \sigma / \partial (1/T) = mQ/R$, where R is the gas constant, this means that the *product* mQ is independent of temperature. Using the above averages m_M and m_S, the following values were obtained: Q_M = 253 kJ/mol and Q_S = 310 kJ/mol.

Table III. Strain rate sensitivity values of the Ni-0.01Nb alloy

Temperature (°C)	m_M (peak stress)	m_S (steady state stress)
800	0.163	0.114
900	0.190	0.142
1000	0.165	0.145
Average	0.173	0.134

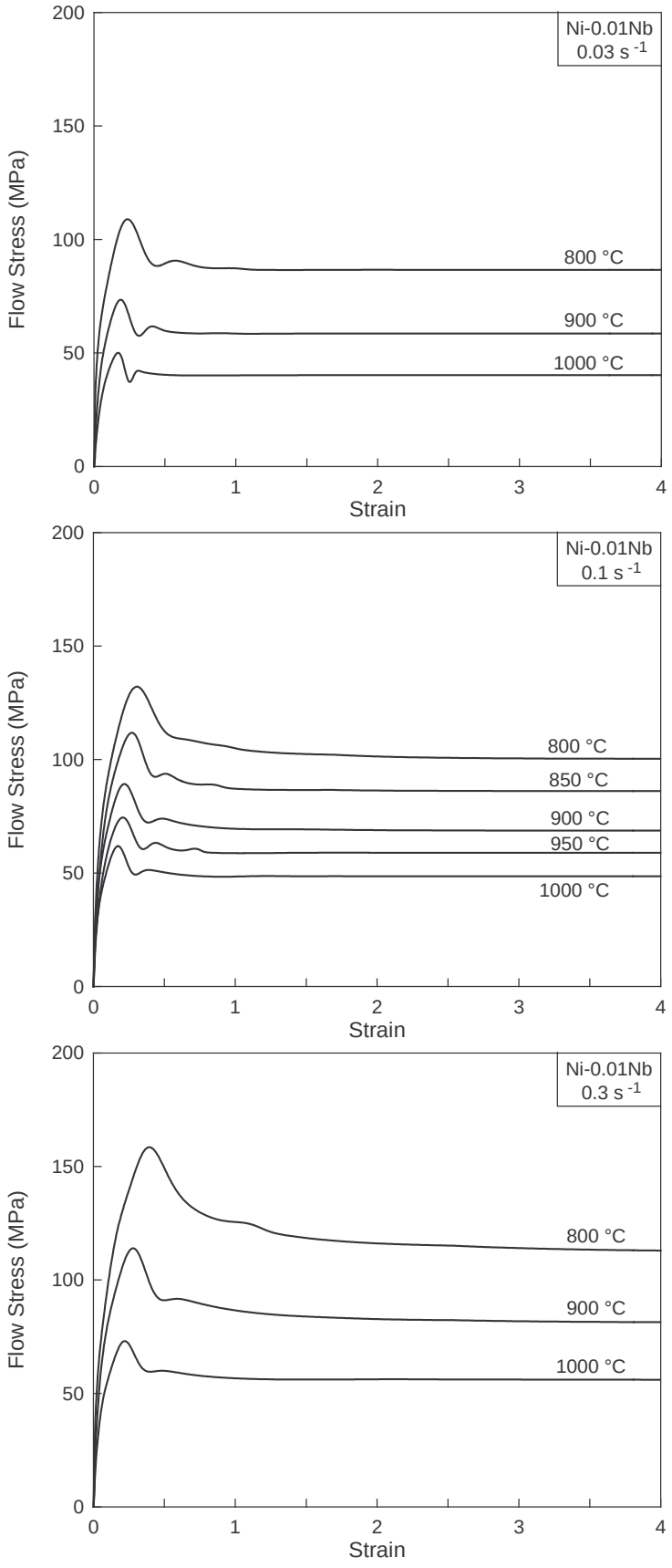

Figure 1. Torsion stress-strain curves of alloy Ni-0.01Nb

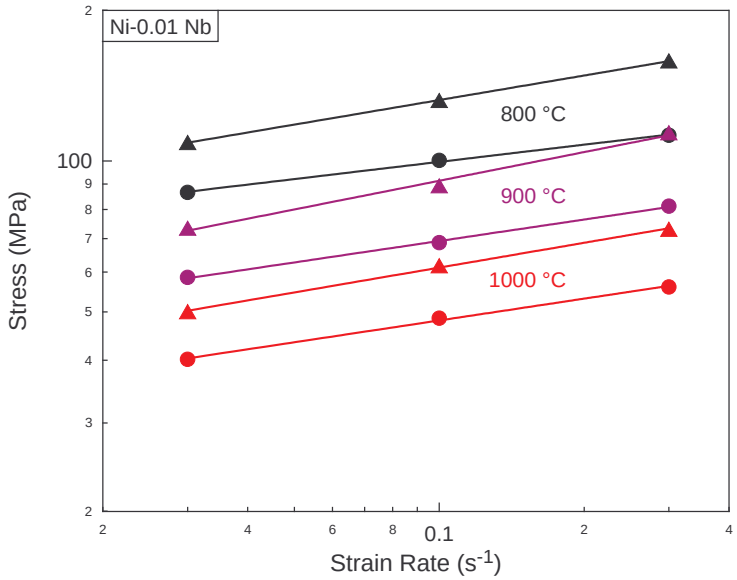

Figure 2. Strain rate dependence of the flow stress of alloy Ni-0.01Nb (triangles: peak stress; circles: steady state stress)

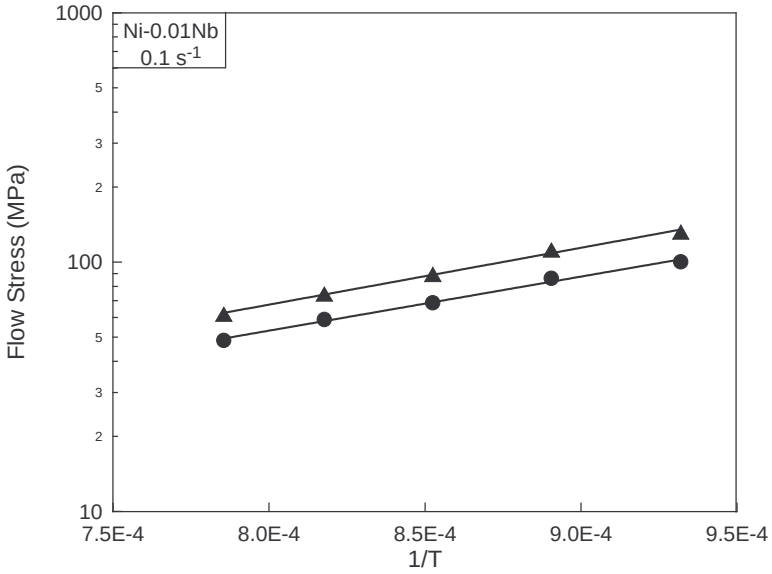

Figure 3. Temperature dependence of the flow stress of alloy Ni-0.01Nb (triangles: peak stress; circles: steady state stress)

III.2. Ni-10Nb Alloy

According to the Ni-Nb phase diagram (see Figure 7), niobium remains entirely in solid solution within the investigated temperature range. As expected, the flow stress level is much higher than for pure nickel or even Ni-1Nb (Figure 4). For instance, at 800 °C and 0.1 s^{-1}, the peak flow stress σ_M = 105 MPa for Ni, 282 MPa for Ni-1Nb and 586 MPa for Ni-10Nb. For that reason, the three flow curves at 800 °C, as well as that at 900 °C–0.3 s^{-1}, are significantly affected by self-heating (fracture of the specimen has even occurred before the end of the test in two cases). Under such straining conditions, only the peak flow stress was therefore considered.

The double logarithmic stress-strain rate plot is shown in Figure 5. The associated values of the strain rate sensitivity parameters m_M (peak stress) and m_S (steady state stress) are reported in Table IV. It is worth to note that m_M increases strongly with temperature, while for m_S the trend is not obvious.

The $\ln\sigma - 1/T$ plots at $\dot{\varepsilon} = 0.1\ s^{-1}$ are shown in Figure 6. Like in the previous cases, the point data are remarkably aligned for both σ_M and σ_S. This means again that the *products* $m_M Q_M$ and $m_S Q_S$ are constant (*i.e.* independent of temperature). A consequence is that Q_M strongly decreases with increasing temperature (Table IV).

Table IV. Strain rate sensitivity and apparent activation energy (at 0.1 s^{-1}) values for the peak stress (m_M, Q_M) and the steady state flow stress (m_S, Q_S) of the Ni-10Nb alloy

Temperature (°C)	$m_M Q_M/R$ (K)	m_M	Q_M (kJ/mol)	$m_S Q_S/R$ (K)	m_S	Q_S (kJ/mol)
800	5872	0.050	977	5069	-	-
900		0.127	385		0.118	357
1000		0.179	273		0.111	380

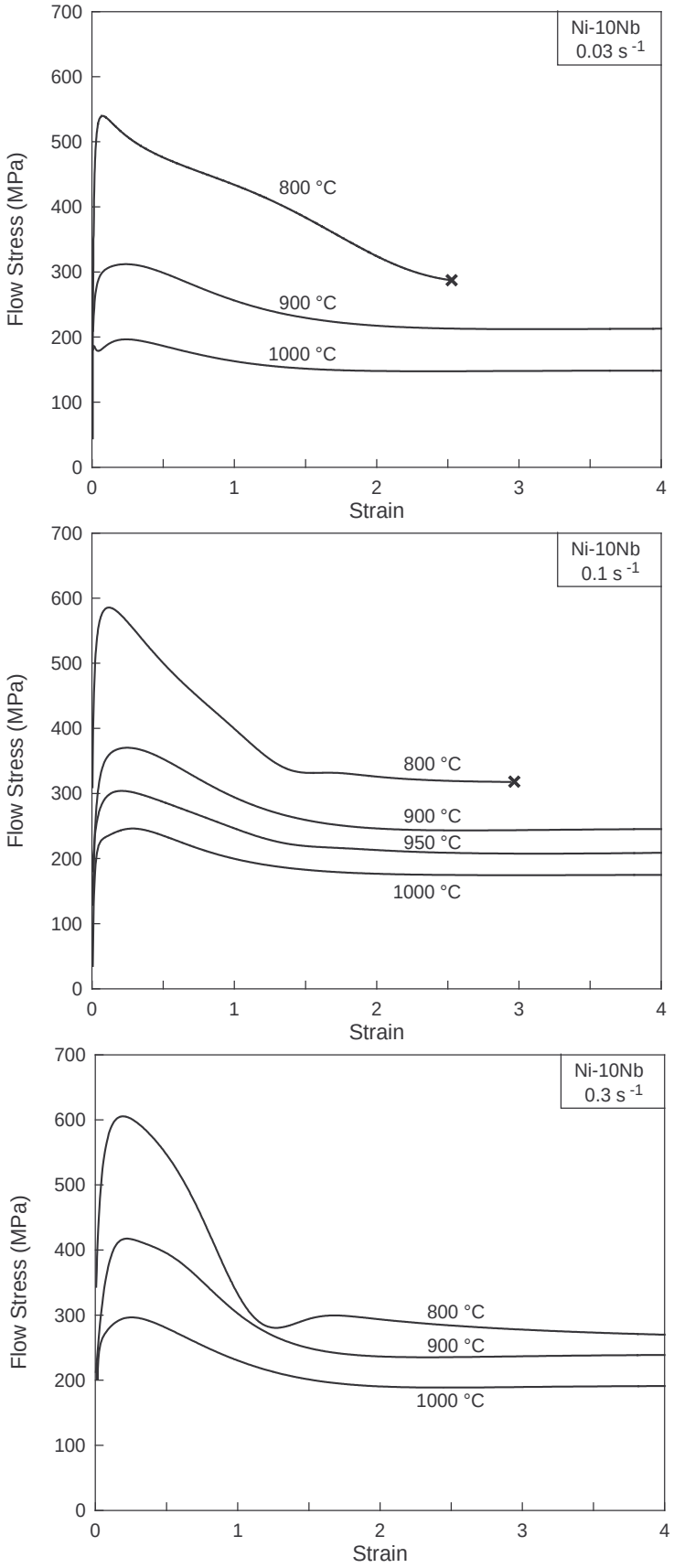

Figure 4. Torsion stress-strain curves of alloy Ni-10Nb (crosses mean fracture)

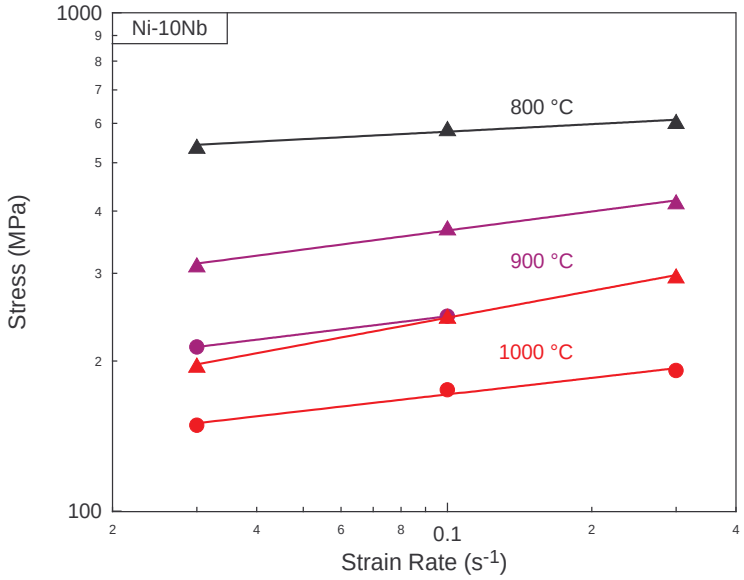

Figure 5. Strain rate dependence of the flow stress of alloy Ni-10Nb (triangles: peak stress; circles: steady state stress)

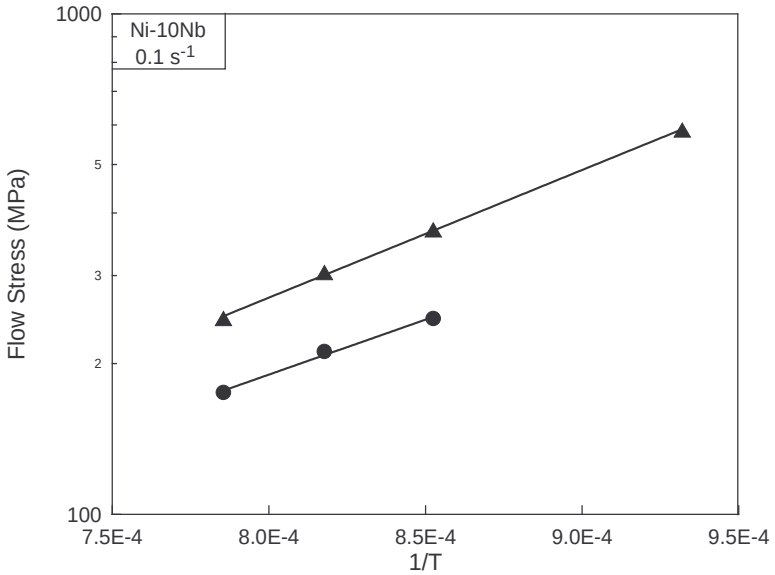

Figure 6. Temperature dependence of the flow stress of alloy Ni-10Nb (triangles: peak stress; circles: steady state stress)

III.3. Ni-15Nb Alloy

The last alloy Ni-15Nb was initially prepared to compare the influence of niobium in solid solution and in the form of intermetallic precipitates (Ni_3Nb) on the hot working behaviour. Since the atomic fraction of niobium is close to 10 %, the phase diagram in Figure 7 shows that precipitation is likely to occur (in static conditions) below 1000 °C. Solid solution annealing for 15 min at 1050 °C was therefore carried out on the specimens, which were then cooled to the deformation temperature. Torsion test were then performed (i) after 10 min holding at the deformation temperature, assuming that no precipitation would take place during this interval; (ii) after 2 h holding in order to produce Ni_3Nb precipitation (see dilatometry data in Section VI.3). Unfortunately, due to the high stress level associated with self-heating, most of the specimens broke at strains less than the scheduled $\varepsilon = 5$ and before a steady state flow stress was reached (Figure 8).

For the above reasons, it was not possible to determine the rheological parameters of this alloy. However, the apparent activation energy can be estimated from the observation that the (steady state) flow stresses are very close in the two straining conditions 900 °C - 0.005 s^{-1} and 1000 °C - 0.1 s^{-1}: identification of the associated Zener-Hollomon parameters leads to $Q \approx 372$ kJ/mol.

The behaviour of this alloy will be discussed below (Section VI) from dilatometry measurements, X-ray diffraction, and electron microscopy observations.

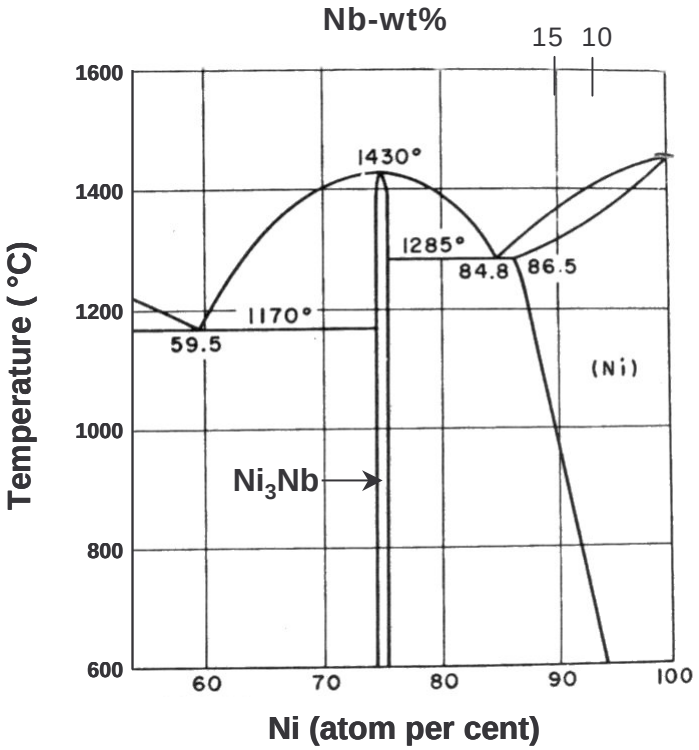

Figure 7. Ni rich part of the Ni-Nb phase diagram

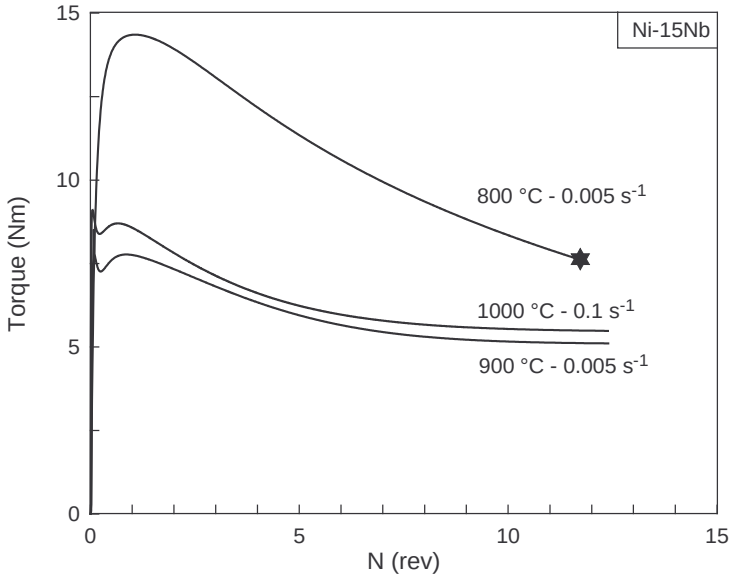

Figure 8. Torque-twist curves of alloy Ni-15Nb (the star means fracture)

IV. QUANTITATIVE ANALYSIS OF THE STRESS-STRAIN CURVES OF Ni-Nb ALLOYS

In this section, the flow curves pertaining to the pure nickel, and alloys Ni-0.01Nb, Ni-0.1Nb, Ni-1Nb, Ni-10Nb are analyzed using the Yoshie-Laasraoui-Jonas (YLJ) flow rule [Yoshie et al., 1987; Laasraoui and Jonas, 1991]. The latter accounts for strain hardening and dynamic recovery, starting from the microscopic equation:

$$\frac{d\rho}{d\varepsilon} = h - r\rho \tag{2}$$

where ρ is the dislocation density, h the strain hardening parameter and r the dynamic recovery parameter. Integration of eq. (2) and combination with the classical relationship $\sigma = \alpha\mu b\sqrt{\rho}$, where $\alpha \approx 1$, μ is the elastic shear modulus and b the Burgers vector modulus, lead to:

$$\sigma = \left\{\sigma_\infty^2 - (\sigma_\infty^2 - \sigma_e^2)\exp\left[-r(\varepsilon - \varepsilon_e)\right]\right\}^{1/2} \tag{3}$$

Here ε_e and σ_e denote the coordinates of a conventional yield point, and $\sigma_\infty = \alpha\mu b\sqrt{h/r}$ is the (virtual) steady state stress level, that would be achieved in the absence of dynamic recrystallization.

For each stress-strain curve, the yield point (ε_e, σ_e) was determined empirically. A numerical procedure was then employed to derive the values of r and σ_∞ giving the best fit of equation (3) with the data. Since dynamic recrystallization is expected to start somewhere before the peak flow stress ($\varepsilon = \varepsilon_M$), only data points for

$\varepsilon < (5/6)\varepsilon_M$ were taken into consideration [Rossard, 1973]. Figure 9 shows a typical example of the results in the case of Ni-0.01Nb deformed at 0.1 s^{-1}. In all cases, the agreement between the data and the YLJ equation is quite good.

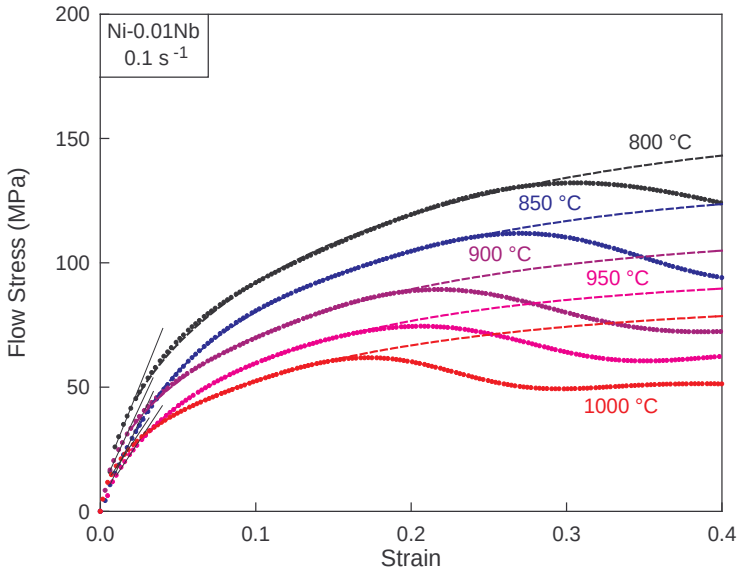

Figure 9. Example showing how the YLJ equation (broken lines) fits the first part (***i.e.***, before the onset of DRX) of the experimental stress-strain curves (dotted lines)

IV.1. Determination of σ_∞ and r

In a first step, each flow curve was associated with the values of r and σ_∞ and the strain rate and temperature dependence of these two parameters was then investigated for the various materials. According to former investigations [Montheillet, 2004], such dependence is expected to be of the form:

$$\sigma_\infty = B\dot{\varepsilon}^{m_\infty} \exp\left(\frac{m_\infty Q_\infty}{RT}\right) \tag{4}$$

and

$$r = r_0\,\dot{\varepsilon}^{-m_r} \exp\left(-\frac{m_r Q_r}{RT}\right) \tag{5}$$

where m_∞ , m_r and Q_∞ , Q_r are the strain rate sensitivities and apparent activation energies associated with σ_∞ and r, respectively, and R is the gas constant. The results are plotted in Figures 10a-d for pure nickel and the four alloys Ni-0.01Nb, Ni-0.1Nb, Ni-1Nb, Ni-10Nb.

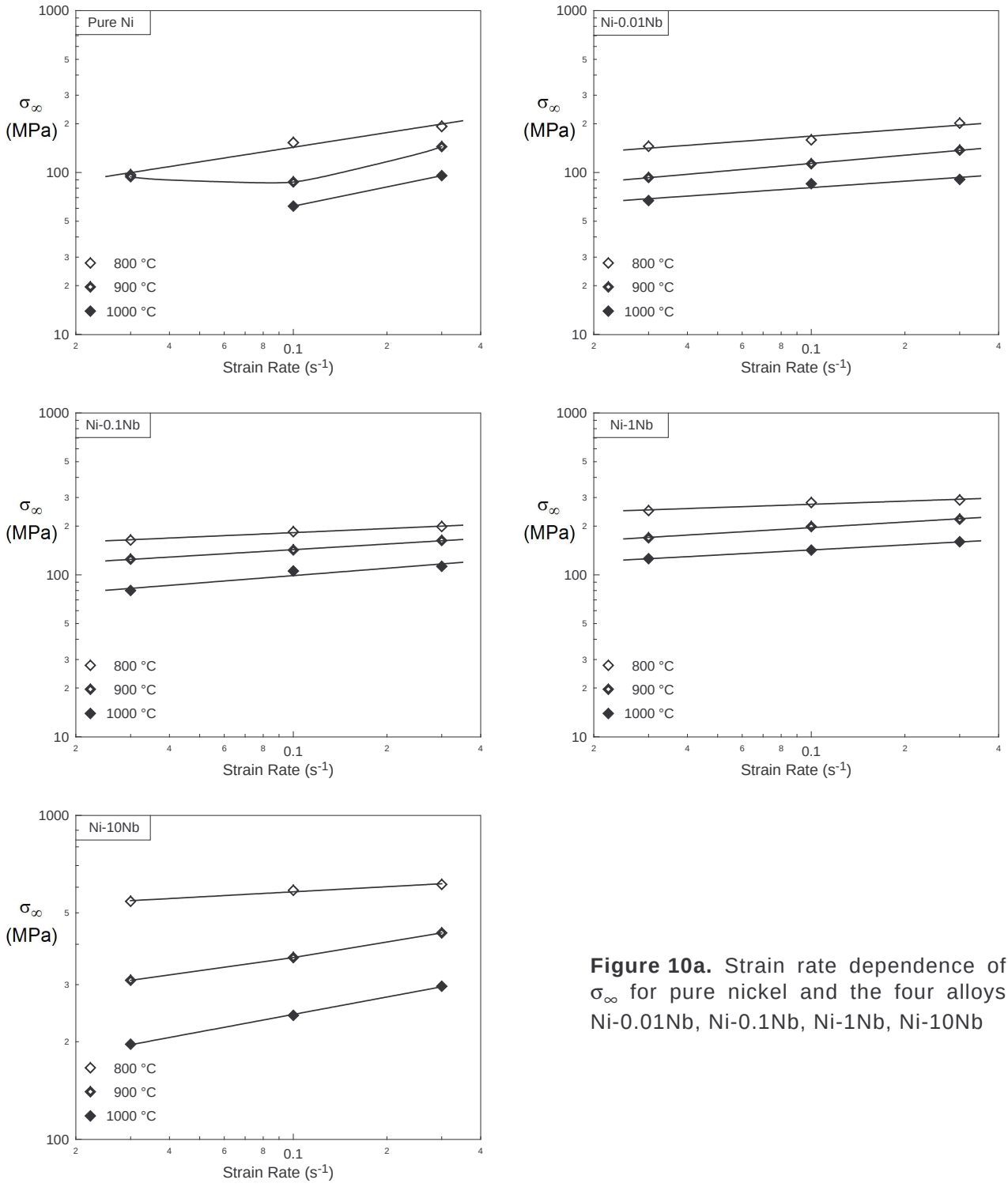

Figure 10a. Strain rate dependence of σ_∞ for pure nickel and the four alloys Ni-0.01Nb, Ni-0.1Nb, Ni-1Nb, Ni-10Nb

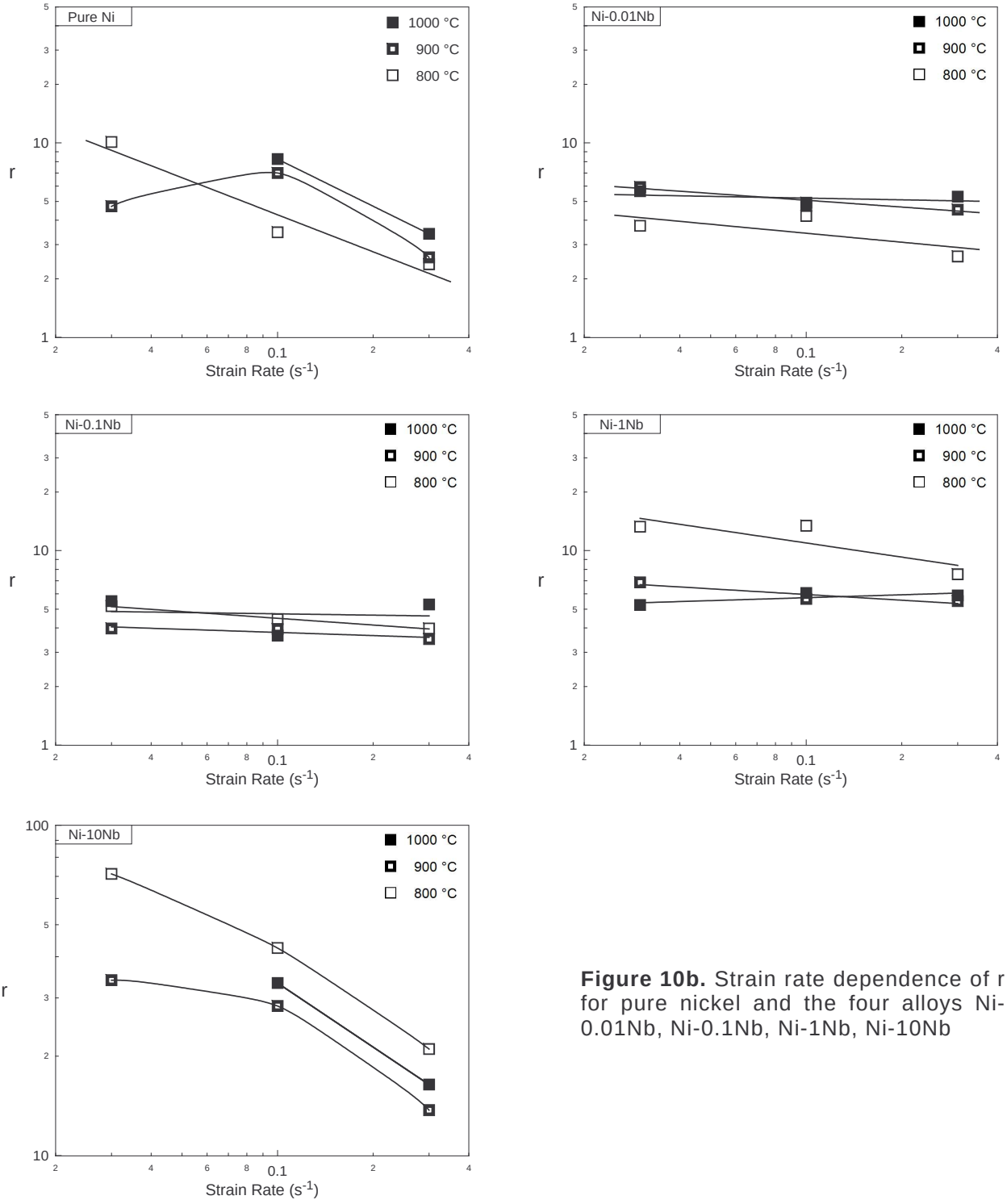

Figure 10b. Strain rate dependence of r for pure nickel and the four alloys Ni-0.01Nb, Ni-0.1Nb, Ni-1Nb, Ni-10Nb

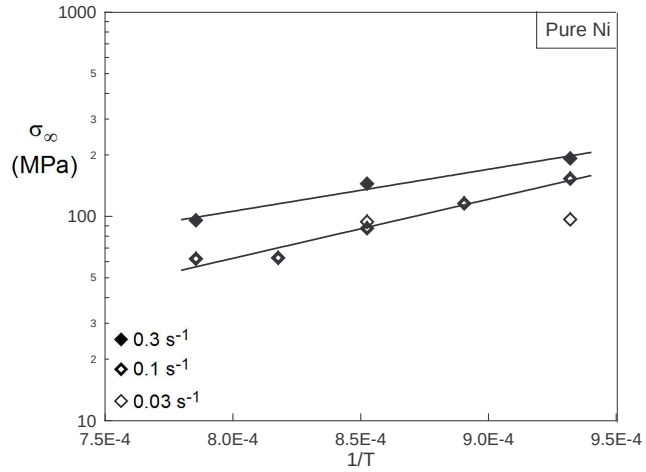

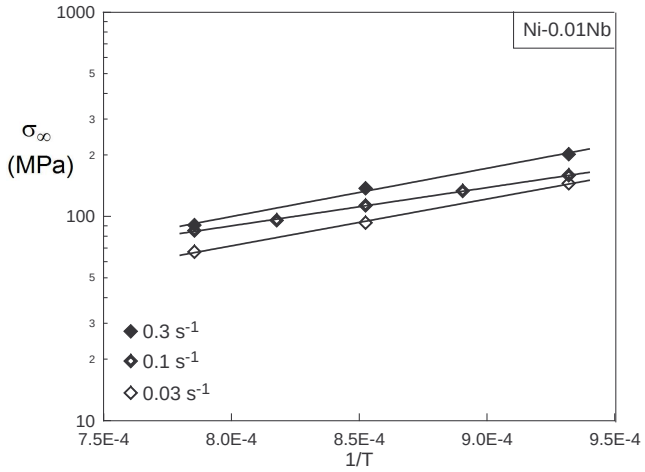

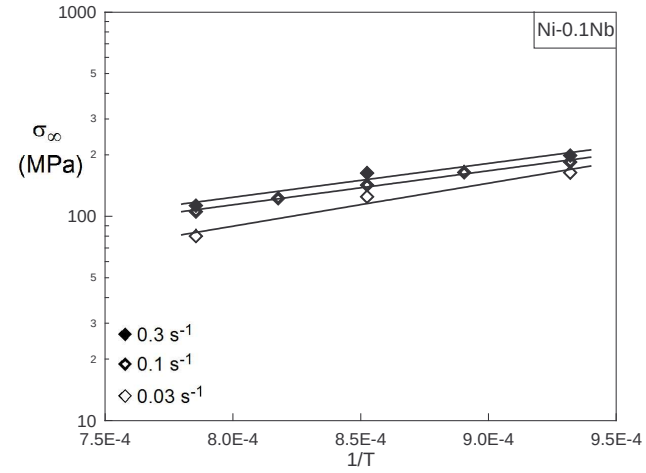

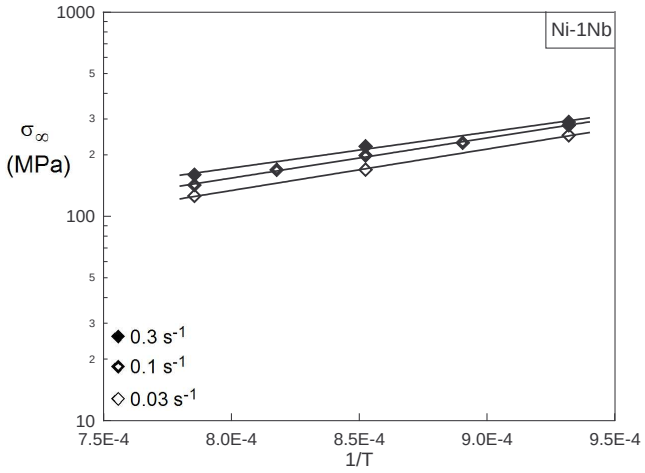

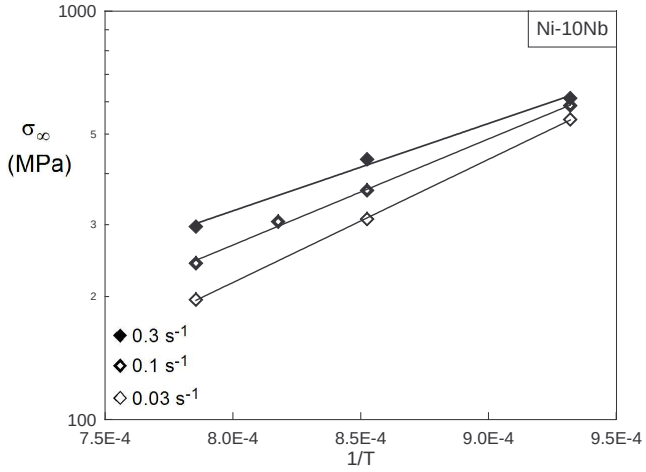

Figure 10c. Temperature dependence of σ_∞ for pure nickel and the four alloys Ni-0.01Nb, Ni-0.1Nb, Ni-1Nb, Ni-10Nb

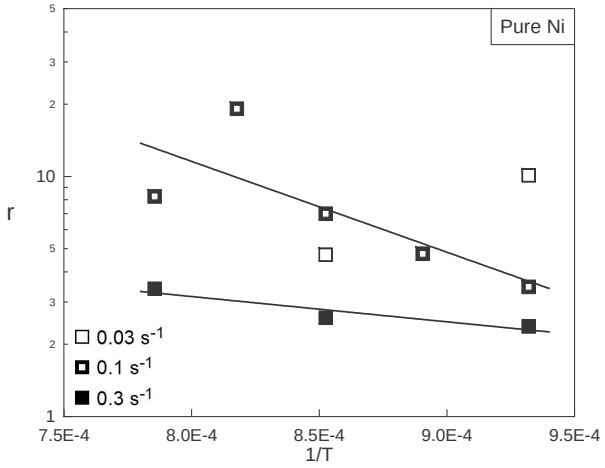

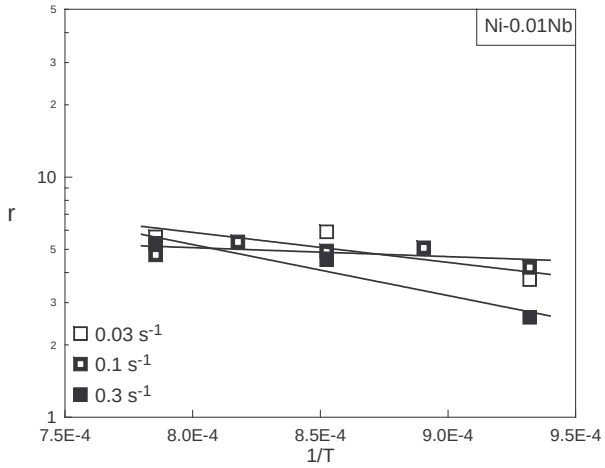

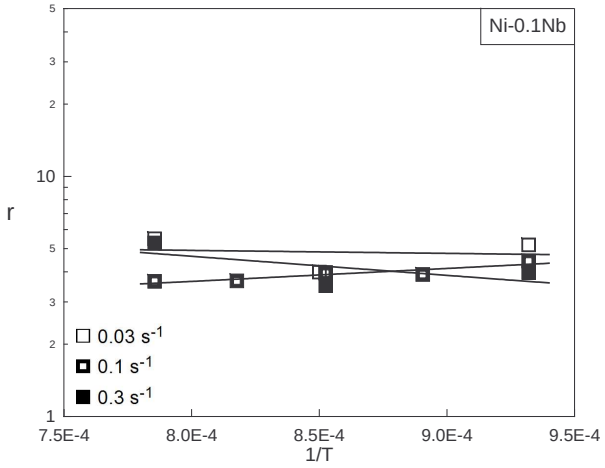

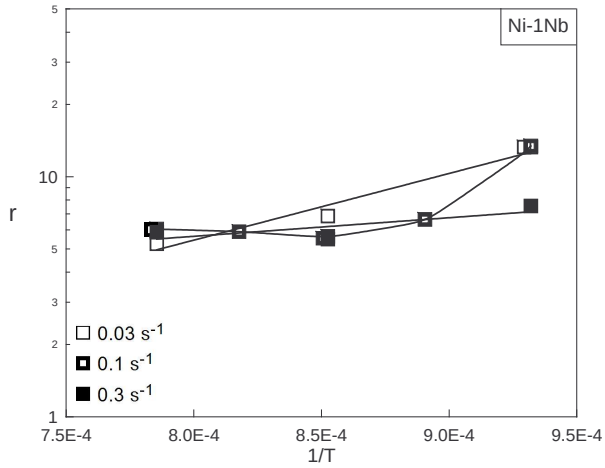

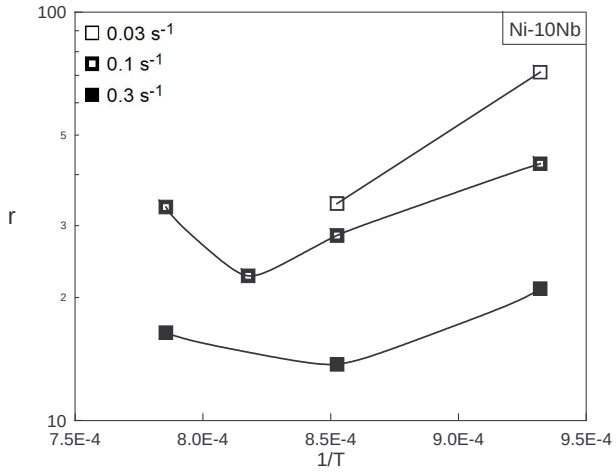

Figure 10d. Temperature dependence of r for pure nickel and the four alloys Ni-0.01Nb, Ni-0.1Nb, Ni-1Nb, Ni-10Nb

The first comments are the following:

a) Strain rate sensitivities: Figure 10a shows that the assumption of a power law relationship dependence of σ_∞ [eq.(4)] is quite correct and the corresponding m_∞ are reported in Table V. The average m_∞ decreases with the addition of niobium. For r, there is more scattering of the data (Figure 10b). However, m_r seems also to drop with an increasing niobium content; for the Ni-0.1Nb, and Ni-1Nb alloys, m_r is quite low, especially at 1000 °C.

Table V. Strain rate sensitivities m_∞ and m_r associated with σ_∞ and r, respectively (brackets indicate estimated values)

	T (°C)	m_∞	m_r
Ni	800	0.300	0.633
	900	[0.458]	-
	1000	[0.395]	0.805
Ni-0.01Nb	800	0.142	0.154
	900	0.169	0.117
	1000	0.132	0.030
Ni-0.1Nb	800	0.084	0.115
	900	0.115	0.054
	1000	0.151	0.023
Ni-1Nb	800	0.066	0.241
	900	0.115	0.097
	1000	0.104	– 0.050
Ni-10Nb	800	0.052	-
	900	0.146	
	1000	0.179	

b) Temperature sensitivities: For σ_∞, the point data are remarkably aligned (Figure 10c), which supports the Arrhenius form of eq.(4). The values of the slope $\bar{m}_\infty Q_\infty / R$ and the associated apparent activation energies Q_∞ are reported in Table VI. Here $\bar{m}_\infty$ denotes the average value of m_∞ over the investigated temperature range, that was used to derive Q_∞. At 0.03 and 0.1 s^{-1}, niobium addition seems to significantly increase Q_∞. However, this trend is not verified at 0.3 s^{-1}, which could be due to self-heating during the tests. For r, the data are again more scattered, but $\bar{m}_r Q_r$ (where $\bar{m}_r$ is the averaged m_r value) globally decays with increasing niobium content, to become close to zero or even negative in Ni-0.1Nb and Ni-1Nb (Figure 10d). Furthermore, m_r is low for these two alloys. It is worth to note that whenever $m_r = 0$, it is not possible to derive any Q_r, which is tantamount to say that the argument $m_r Q_r$ of the exponential in eq.(4) is not relevant in such a case. For the last alloy Ni-1Nb, the variations of $\bar{m}_r Q_r$ are not monotonic over the investigated temperature range, such that Q_r was not determined.

IV.2. Determination of h

The strain hardening parameter h was determined in a second step from its definition:

$$\sigma_\infty = \alpha \mu b \sqrt{h / r} \qquad (6)$$

where α was assumed to equal unity, and $b = 2.49 \times 10^{-10}$ m (pure nickel). The elastic shear modulus μ was in turn determined as a function of temperature from the following equation [Frost and Ashby, 1982]:

$$\mu = \mu_0 \left(1 + \eta \frac{T - 300}{T_M} \right) \qquad (7)$$

with, to a first approximation, $\mu_0 = 7.89 \times 10^4$ MPa (for Ni at 300 K), $T_M = 1726$ K (Ni), and $\eta = -0.64$.

The values are displayed in Figure 11 in an h-r diagram for comparison of the five materials investigated. It is interesting to note that r is ranging roughly between 2 and 10 for pure nickel and the low alloy materials (up to 1 %Nb), which is to be compared with the value $r \approx 5$ recently found for a model alloy close to 304 stainless steel [Gavard, 2001]. Such low value is likely to reflect the weak recovery capacity of low stacking fault energy materials. By contrast, Ni-1Nb displays much higher r-values. However, the latter are not likely to reflect a more efficient dynamic recovery in this alloy, but rather the fact that the flow stress level is partly governed by solute drag, instead of dislocation density. Figure 11 also shows that the strain hardening parameter h is not sensitive to niobium solutes up to 0.1 %, but increases significantly for Ni-1Nb and Ni-10Nb.

Table VI. Temperature dependence parameters associated with σ_∞ and r (brackets indicate estimated values)

	$\dot{\varepsilon}(s^{-1})$	$\bar{m}_\infty Q_\infty / R$ (K)	Q_∞ (kJ/mol)	$\bar{m}_r Q_r / R$ (K)	Q_r (kJ/mol)
Ni	0.03	-	-	-	
	0.1	6654	[144]	8706	101
	0.3	4730	[102]	2423	28
Ni-0.01Nb	0.03	5275	297	2880	239
	0.1	4312	243	861	71
	0.3	5440	307	4898	406
Ni-0.1Nb	0.03	4845	346	287	37
	0.1	3836	274	– 1246	– 162
	0.3	3816	272	1826	237
Ni-1Nb	0.03	4667	409	– 6394	– 554
	0.1	4517	396	-	-
	0.3	4035	353	– 1782	– 154
Ni-10Nb	0.03	6941	460	-	
	0.1	5975	396		
	0.3	4922	326		

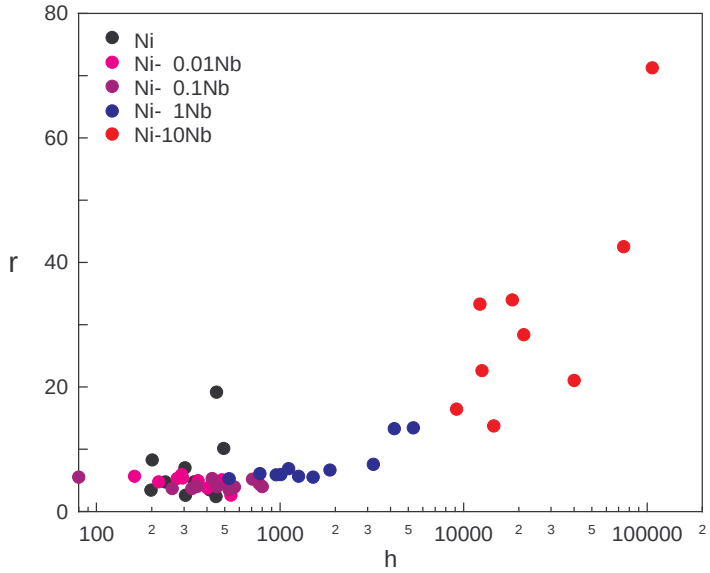

Figure 11. Diagram showing the h and r values of the five materials investigated

IV. STEADY STATE STRESS *VS.* GRAIN SIZE RELATIONSHIP

A number of authors have found an inverse power law relationship between the steady state flow stress and the average steady state grain (or crystallite) size:

$$\sigma_s = K / \bar{D}^a \qquad (8)$$

with an exponent a generally ranging between 0.6 and 0.8 [Derby, 1992].

Metallographic observations were carried out on the four grades Ni, Ni-0.01Nb, Ni-0.1Nb, and Ni-1Nb deformed to a strain of 5 (≈ steady state) at the three temperatures 800, 900, and 900 °C for $\dot{\varepsilon} = 0.1\,s^{-1}$. Metallographic preparation of the specimens involved mechanical polishing up to 3 µm, electrolytic polishing, and chemical etching ($CuCl_2$ solution). A quantitative analysis software was used to determine the mean equivalent circle diameter (ECD) of the grains, considered here to be representative of the average grain size.

The results are displayed in Figure 12, together with some EBSD data points obtained previously (in the latter case, the grain size was identified to the mean intercept of boundaries associated with a misorientation angle larger than 15 deg). The values of the exponent a are reported in Table VII. For Ni and the alloys Ni-0.01Nb and Ni-0.1Nb, a is slightly less than usually reported, while the value a = 1.35 for Ni-1Nb (optical microscopy) is much larger. However, EBSD data lead to a = 0.58 for the same alloy, which seems to be more reliable. Unexpectedly, the diagram shows that for a given grain size, the flow stress *decreases* with increasing niobium content. This suggests that the hardening effect of niobium in solid solution is basically related to grain refinement. Finally, it is worth to note that when the (OM) data pertaining to the various materials are considered together (broken line), a

takes the value 0.33, which is quite smaller than that obtained by Derby [1992], who considered a set of data relative to various industrial alloys.

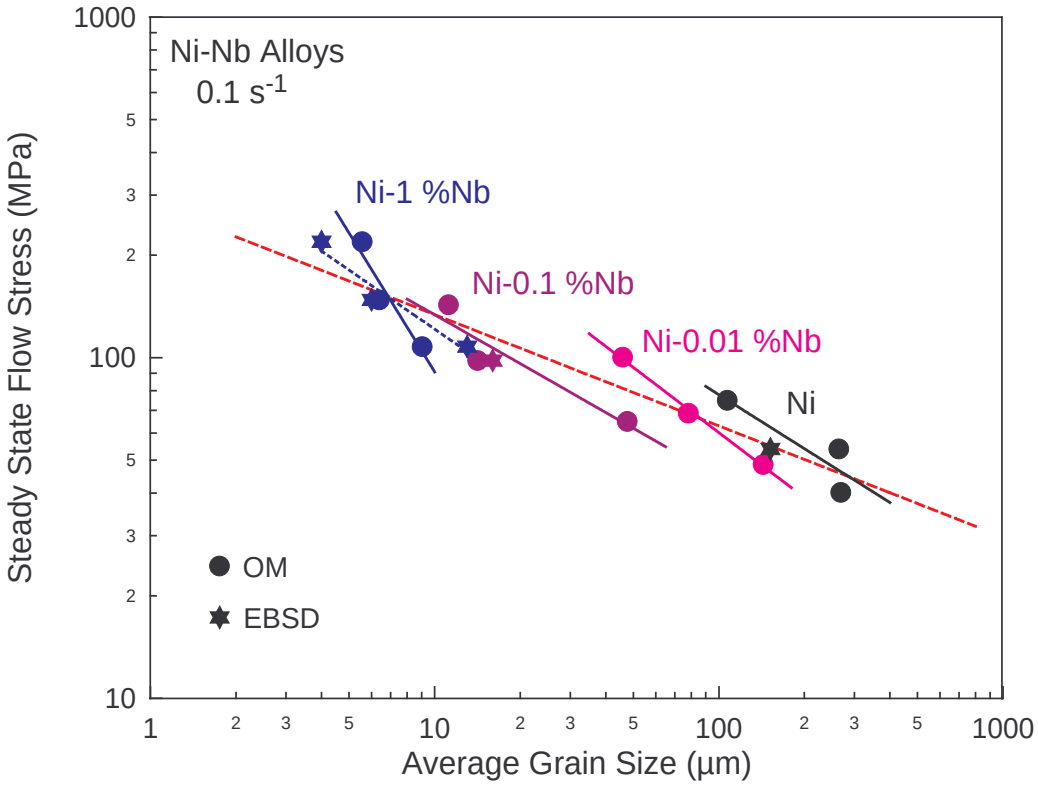

Figure 12. Diagram showing the relationship between steady state flow stress and average grain size. Optical microscopy (OM) and EBSD data. The broken line fits the whole set of OM data.

Table VII. Exponent a of the steady state flow stress ***vs.*** grain size relationship (OM: optical microscopy)

	a
Ni (OM)	0.53
Ni-0.01Nb (OM)	0.64
Ni-0.1Nb (OM)	0.48
Ni-1Nb (OM)	1.35
Ni-1Nb (EBSD)	0.58
All OM data	0.33

VI. DISCUSSION

Putting together the above results and that previously obtained [Montheillet et al., 2004] allows the influence of niobium solutes on the hot deformation of nickel to be analyzed.

VI.1. Solid solution hardening

Both the peak flow stress σ_M and the steady state flow stress σ_S increase very rapidly with the niobium content, as illustrated by Figure 13 for pure nickel and the four Ni-Nb alloys. In spite of data scattering, the following power law dependence of the flow stress is confirmed:

$$\sigma = \sigma_0 + k\, x^p \qquad (9)$$

where x is the solute content (wt%) and p ranges from 0.37 to 0.43. Such hardening law is different from the classical linear dependence frequently reported in the literature (for larger solute contents) at room temperature. It should be kept in mind, however, that hot deformation is addressed here and that σ_M and σ_S are likely to be influenced by the initial grain size and the steady state grain size, respectively. Both are expected to decrease with increasing x, and therefore contribute to hardening. In fact, it has been shown in the previous section that the flow stress hardening by niobium in nickel is due to grain refinement rather than to direct solute effects.

VI.2. Strain rate and temperature dependence of the flow stress

Figure 14 shows the influence of niobium concentration on the product mQ, and the classical rheological parameters m and Q considered separately. The product mQ clearly goes through a maximum at low niobium concentrations, but increases again for Ni-10Nb. By contrast, m and Q are monotonic decreasing and increasing functions of the niobium content, respectively, although the trend is not exactly confirmed for Ni-10Nb. The influence of niobium is strong but appears to become much less efficient at concentrations larger than 0.1 wt%. These observations suggest that the mechanism controlling the flow stress level is not the same at low (< 0.1 %) and large (≥ 10 %) niobium concentrations.

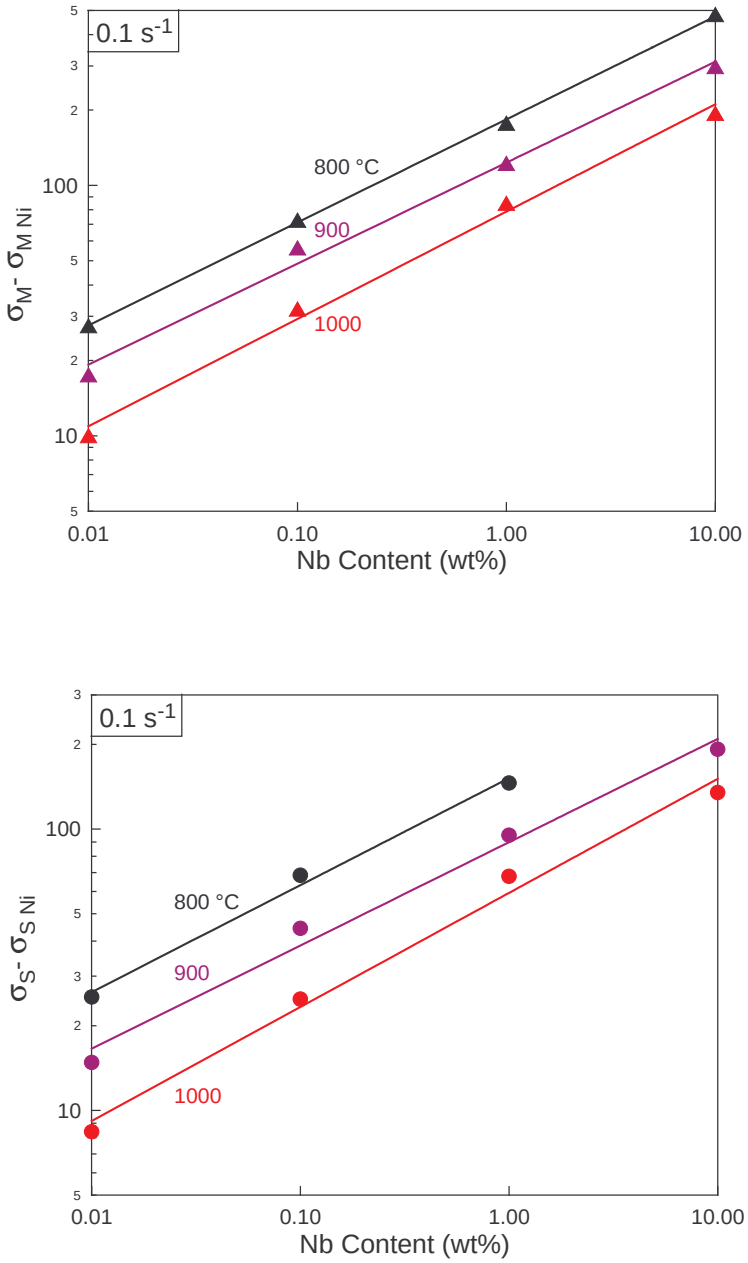

Figure 13. Influence of niobium content on the peak and steady state flow stresses of pure nickel and the Ni-Nb alloys at various temperatures and a strain rate of 0.1 s^{-1}

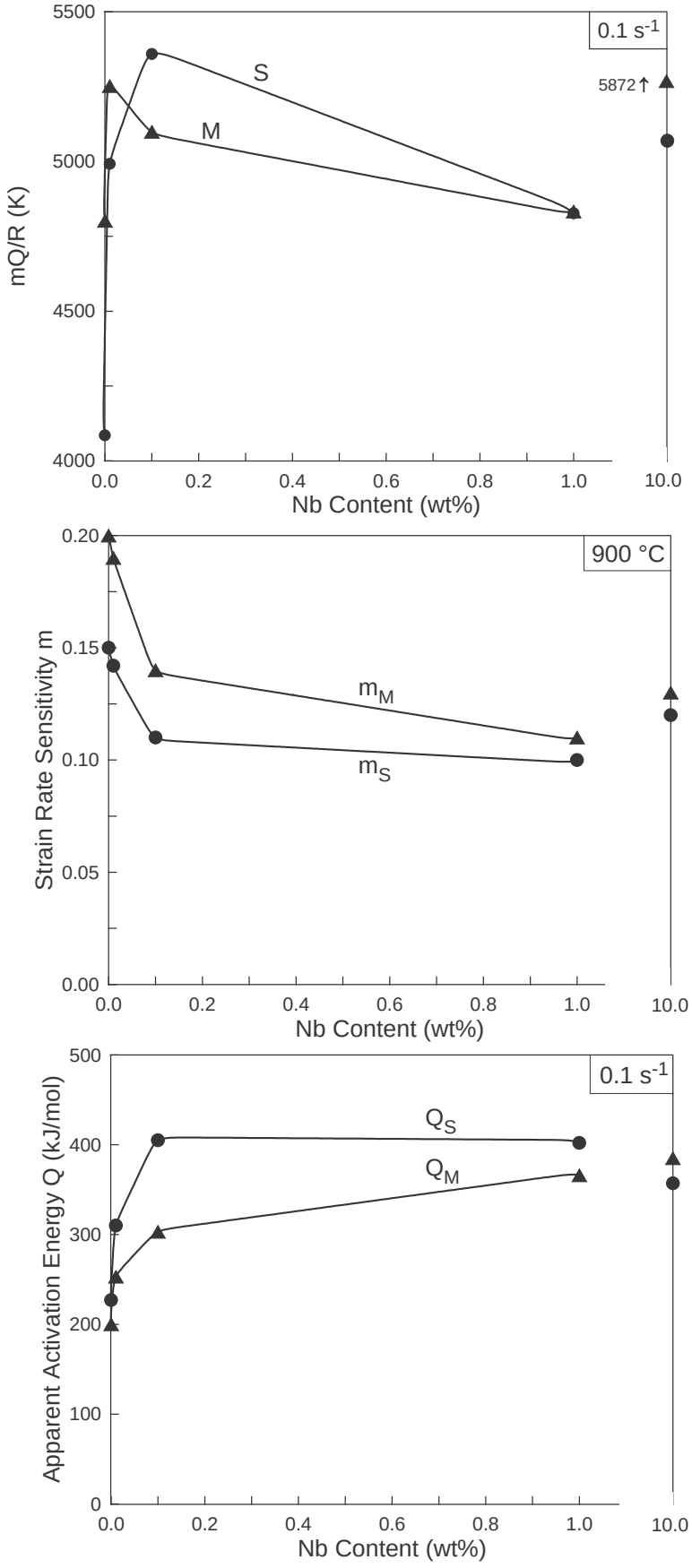

Figure 14. Influence of the solute niobium content on mQ, m and Q (M: peak stress; S: steady state stress)

VI.3. Behaviour of the Ni-15Nb alloy

Three types of observation were used to check if intermetallic precipitates were present before and/or after deformation in the alloy Ni-15Nb (see Section III.3 above). First, dilatometry measurements were carried out on pure nickel at 800 °C, and on the Ni-15Nb alloy at 1000, 900, 800, and 700 °C. In each case, the specimen was first annealed for 1 h at 1050 °C to ensure complete dissolution of niobium precipitates, and then slowly cooled to the selected temperature. Isothermal length changes of the specimen were then recorded. Figure 15 exhibits monotonic contractions for Ni-15Nb at 1000 °C and 900 °C, as well as for pure nickel at 800 °C. By contrast, for Ni-15Nb at 800 °C and 700 °C, the inverse trend is observed after about 25 min holding at the test temperature (after the cooling time). Such behaviour is likely to reflect intermetallic precipitation, in agreement with the phase diagram of Figure 7. Furthermore, at given temperature, the latter appears to be much slower than in industrial alloys.

X-ray diffraction measurements were then performed on specimens of Ni-15Nb after various holding times at 800 °C (15 min and 120 min) and 900 °C (10 min), as well as on a torsion specimen strained to $\varepsilon = 5$ at 900 °C and 5×10^{-3} s^{-1}. In all cases, there was no evidence of precipitation. Furthermore, the lattice parameter was close to 0.359 nm, which corresponds to a Ni-Nb solid solution containing about 10 at%Nb [Pearson, 1964].

Finally, transmission electron microscopy observations were carried out on the same specimens as above. In all cases, diffraction patterns exhibited only spots associated with the nickel matrix, and no precipitates could be identified on the bright field images.

It can therefore be concluded that if intermetallic precipitates (Ni_3Nb) are present in the Ni-15Nb alloy, they must be ultrafine. Their volume fraction is likely to be low, since the matrix parameter indicates a solute content close to 10 at%. Furthermore, dilatometric measurements show that, if precipitation really occurs, its kinetics must be quite slow.

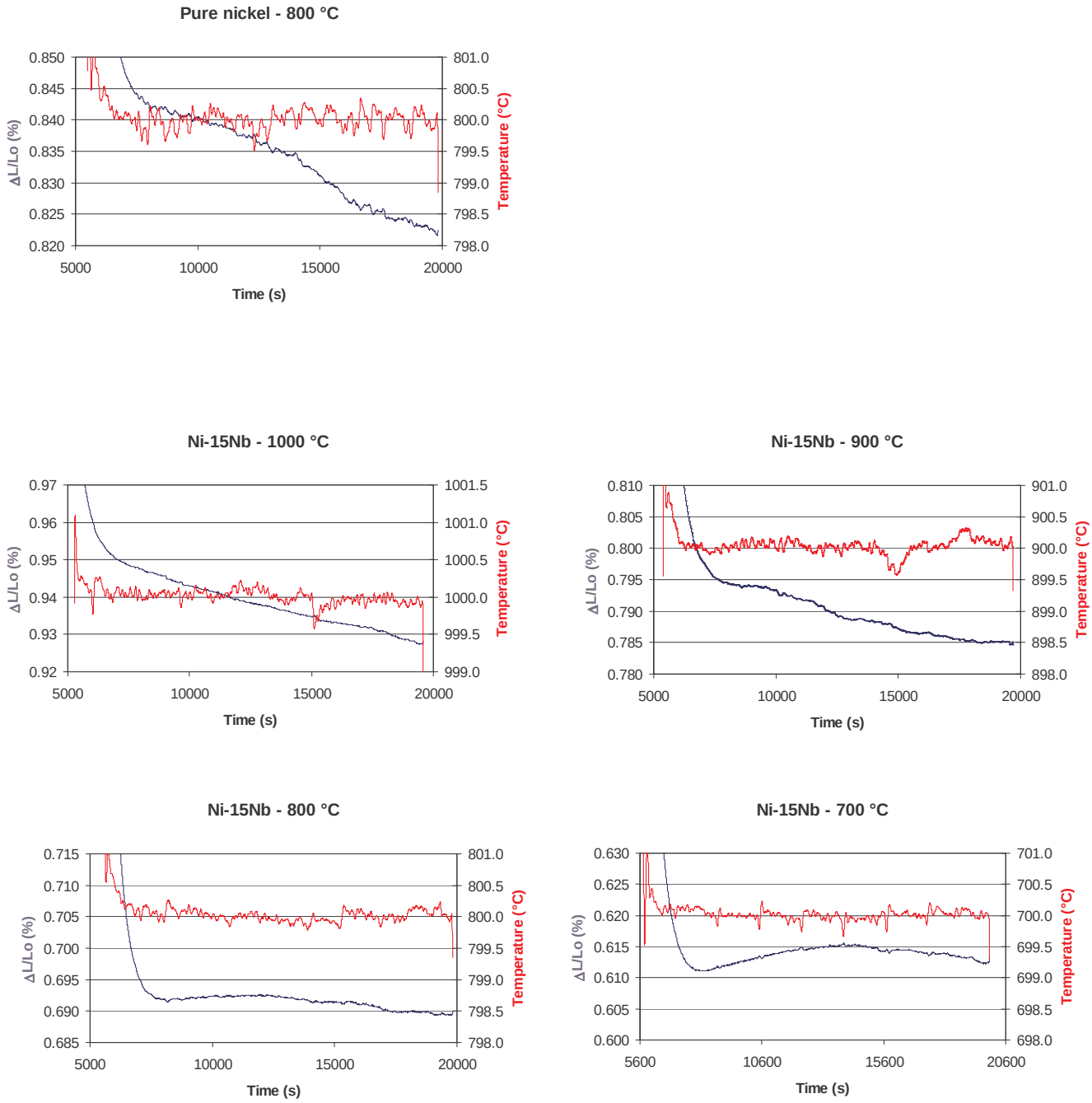

Figure 15. Dilatometry measurements carried out on pure nickel at 800 °C and on alloy Ni-15Nb at 1000, 900, 800, and 700 °C

V. CONCLUSIONS AND FUTURE DEVELOPMENTS

The results reported above have to be combined with that presented in a previous report [Montheillet et al., 2004]. They contribute to the knowledge of the influence of niobium (mostly in solid solution) during hot working of Ni base alloys:

(i) Niobium solutes increase the peak and steady state flow stresses quite efficiently according to a power law relationship $\sigma = \sigma_0 + k\,x^p$, where x is the niobium content (wt%) and p is close to 0.4.
Such effect, however, is apparent, in the sense that the flow stress level also depends on the initial and steady state grain sizes, respectively. In particular, in the case of the steady state flow stress, it has been shown that the hardening effect of niobium solutes is *indirect*, since it is entirely due to grain size refinement.

(ii) For all materials, the $\ln\sigma - (1/T)$ plots are perfectly linear, which means that the product mQ is independent of temperature, although m and Q taken separately are not. Niobium solutes decrease the strain rate sensitivity of the flow stress and increase the apparent activation energy. Such effects are quite strong for low (< 0.1 wt%) niobium contents but saturate at larger concentrations.

(iii) A quantitative analysis of the flow rules using the Yoshie-Laasraoui-Jonas equation led to the determination of the rheological parameters σ_∞, h and r. The first one denotes the steady state flow stress in the absence of dynamic recrystallization, whereas h depicts the kinetics of strain hardening, and r the kinetics of dynamic recovery (for low alloy materials). These parameters allow to quantify the material behaviour, and can be used to analyze the effect of niobium on the various elementary mechanisms of hot deformation. In particular, they are likely to reflect the possible change of controlling mechanism with increasing niobium content.

(iv) Finally, it was shown that intermetallic precipitation in the Ni-15Nb alloy -if it occurs- should be very fine and associated with slow kinetics. Since it was not possible to determine the rheological parameters of this alloy, the question of the influence of precipitation on the hot working behaviour is still open. However, the present data show that binary Ni-Nb alloys are good model materials for such investigations, since Ni_3Nb precipitation is much slower than in industrial alloys such as IN 718.

Short-term developments of this research would aim at completing our knowledge of the hot working behaviour and mechanisms of the binary Ni-Nb alloys. This would include a more detailed investigation of the respective influences of niobium solutes and grain size (*i.e.*, initial or resulting from dynamic recrystallization) on the flow stress levels and the associated rheological parameters. For that purpose, new optical metallography and EBSD observations should be carried out on the deformed specimens of the various alloys. It would also be useful to investigate the deformation textures, that are likely to influence the steady state flow stress.

Since the results obtained on binary Ni-Nb alloys were partly unexpected, it would be interesting, as longer-term perspective, to analyze the hot working

behaviour of a model material closer to the classical nickel base superalloys (such as IN 718), starting from a Ni-Cr or Ni-Cr-Fe base with controlled additions of niobium.

References

Derby B. Dynamic recrystallization: the steady state grain size. *Scripta Metall.* **27**, 1581-1585 (1992).

Frost H.J. and Ashby M.F. Deformation-mechanism maps. The plasticity and creep of metals and ceramics, Pergamon Press (1982).

Gavard L. Recristallisation dynamique d'aciers inoxydables austénitiques de haute pureté. *Ph.D. Thesis*, Ecole des Mines de Saint-Etienne (2001).

Laasraoui A. and Jonas J.J. Prediction of steel flow stresses at high temperatures and strain rates. *Mater. Sci. Technol.* **7,** 78-82 (1991).

Le Coze J., Tardy R., Kobylanski A. and Biscondi M. Preparation of high purity metals and metallurgical studies at the Ecole des Mines from 1970. Review. *Proc. 1st Int. Conf. on Ultra High Purity Base Metals (UHPM-94)*, Kitakyushu-City, Japan, Japan Institute of Metals, p.371-389 (1995).

Montheillet F., Girard-Insardi S., Desrayaud Ch. and Le Coze J. Influence of niobium on the dynamic recrystallization of nickel. EOARD Contract No. FA8655-03-M-4061, Final Report (2004).

Montheillet F., Girard S., Desrayaud Ch., Semiatin S.L. and Le Coze J. Hot working of high purity base nickel-niobium alloys. Int. Conf. on Processing and Manufacturing of Advanced Materials (THERMEC'2006), Vancouver, BC, Canada (2006), *in press.*

Pearson W.B. A handbook of lattice spacings and structures of metals and alloys, Pergamon Press (1964).

Rossard C. Mechanical and structural behaviour under hot working conditions. *Proc. 3rd Int. Conf. on the Strength of Metals and Alloys*, Institute of Metals (London), Monogr. Rep. Ser. n° 36, Cambridge, p.175-203 (1973).

Yoshie A., Morikawa H., Onoe Y. and Itoh K. Formulation of static recrystallization of austenite in hot rolling process of steel plate. *Trans. ISIJ* **27**, 425-431 (1987).